Research in Astronomy and Astrophysics, 25:104006 (14pp), 2025 October
https://doi.org/10.1088/1674-4527/adf715
CSTR: 32081.14.RAA.adf715
© 2025. National Astronomical Observatories, CAS and IOP Publishing Ltd. All rights, including for text and data mining, AI training, and similar technologies, are reserved.

Cycle-CNN: A Method for Measuring Stellar Atmospheric Parameters from Low-resolution and Low-SNR LAMOST Spectra

Ming-Lei Wu[1], Yuan Liu[1], and Yu-De Bu[2]
[1] School of Computer Science and Technology, Shandong Technology and Business University, Yantai 264005, China
[2] School of Mathematics and Statistics, Shandong University, Weihai 264200, China; buyude@sdu.edu.cn
Received 2025 April 21; revised 2025 July 10; accepted 2025 July 21; published 2025 September 12

Abstract

Compared to high-resolution spectra, low-resolution spectra offer higher observational efficiency and broader sky coverage, making them especially valuable for large-scale stellar surveys. The Large Sky Area Multi-Object Fiber Spectroscopic Telescope (LAMOST) survey alone has collected tens of millions of low-resolution stellar spectra, providing an unprecedented opportunity for large-scale stellar parameter estimation. However, a substantial portion of these spectra suffer from low signal-to-noise ratio (low-SNR), which poses significant challenges for accurate parameter determination. Accurately extracting stellar atmospheric parameters from such data can significantly enhance the utility of spectral observations. However, these low-SNR spectra often introduce considerable uncertainty in parameter estimation. To address this issue, we propose a novel method based on the Cycle-Consistent Convolutional Neural Network (Cycle-CNN) for predicting key stellar atmospheric parameters, including effective temperature ($T_{\rm eff}$), surface gravity ($\log g$), and metallicity ([Fe/H]). This method integrates the cycle-consistency learning mechanism of Cycle-GAN with the strong modeling capability of CNNs, thereby improving model robustness and reducing prediction uncertainty under low-SNR conditions. We train and evaluate the model on spectra from LAMOST DR9 across different SNR intervals (2–15). For spectra with SNR between 10 and 15, the model achieves prediction accuracies of 63.22 K for $T_{\rm eff}$, 0.11 dex for $\log g$, and 0.07 dex for [Fe/H]. For the spectra with SNR between 5 and 10, the prediction accuracies are 89.45 K, 0.17 dex, and 0.11 dex, respectively. Even under extreme conditions with SNR between 2 and 5 and limited data availability, the model maintains good performance, achieving accuracies of 145.36 K, 0.29 dex, and 0.18 dex. Furthermore, we validate our predictions against reference parameters from high-resolution surveys, and the results demonstrate good consistency with other large-scale spectroscopic surveys. These findings indicate that the proposed Cycle-CNN method can provide stable and accurate predictions of atmospheric parameters even under low-quality spectral conditions, offering a reliable solution to improve the scientific utilization of low-quality spectra.

Key words: surveys – techniques: spectroscopic – methods: data analysis

1. Introduction

The measurement of stellar atmospheric parameters is of vital importance in astronomy, as it helps to gain a deeper understanding of the physical properties, evolutionary histories, and roles of stars in the Universe. Stellar atmospheric parameters include effective temperature ($T_{\rm eff}$), surface gravity ($\log g$), metallicity ([M/H]) and rotational velocity ($v \sin i$). These parameters not only reveal fundamental physical characteristics of stars but also provide critical insights into their formation environments, chemical compositions, and evolutionary states (Ho et al. 2017). Accurate determination of stellar atmospheric parameters enables astronomers to infer stellar ages, masses, and evolutionary phases, thereby supporting the development of stellar evolution theories. Moreover, parameters such as metallicity reflect the chemical composition of the interstellar medium, contributing to our understanding of the chemical evolution of the Milky Way and other galaxies. For instance, stellar metallicity is closely related to planet formation; stars with higher metallicities are more likely to host terrestrial planets. In the study of galactic evolution, stellar atmospheric parameters facilitate the construction of stellar population models, which in turn help reveal the structure and dynamics of galaxies. Furthermore, these parameters play a crucial role in cosmic distance measurements. Accurate estimation of stellar luminosities improves the precision of cosmic distance scaling. Through such measurements, astronomers can better understand the interplay between stars and planetary systems, thus advancing the fields of planetary science and the study of the interstellar medium.

1.1. Large-scale Surveys and Data Characteristics

Large-scale spectroscopic surveys have become core tools in modern astronomical research. Through extensive observations and data collection, these surveys provide invaluable

resources for in-depth studies of stars, galaxies, and cosmology. International collaborative projects such as Large Sky Area Multi-Object Fiber Spectroscopic Telescope (LAMOST), SDSS, Gaia, and TESS have achieved significant results in various fields. LAMOST has collected a vast amount of stellar spectra, offering crucial insights into the structure of the Milky Way, stellar atmospheric parameters, and chemical evolution, despite the challenge of low-quality spectra (Luo et al. 2015). SDSS, utilizing high-resolution spectra, has constructed a three-dimensional (3D) map of the Universe and contributed large data sets for quasar and galaxy studies (York et al. 2000). Gaia provides high-precision astrometric and kinematic data, revealing the spatial distribution and dynamics of stars in the Milky Way (Prusti et al. 2016). TESS focuses on the detection of exoplanets and also delivers rich time-domain data for stellar variability studies (Ricker et al. 2015). Other surveys such as APOGEE and DESI have made important contributions to Galactic chemical evolution and large-scale structure research (DESI Collaboration et al. 2016; Majewski et al. 2017). Although these projects face challenges in data processing and storage, the advancement of machine learning and big data technologies offers promising solutions for low-quality spectra and large-scale data analysis, further promoting innovation and development in astronomy.

High-resolution spectroscopy, due to its superior precision, can resolve fine spectral features and thus provides higher accuracy in measuring stellar physical parameters. This makes it particularly valuable for in-depth analysis of detail-rich astrophysical objects, including stars, massive galaxies, and planetary atmospheres. However, longer exposure times and higher demands on data processing and storage make high-resolution spectroscopy less efficient in large-scale sky surveys. In contrast, low-resolution spectroscopy offers shorter exposure times and higher data processing efficiency, making it well-suited for large-scale astronomical surveys. Although it lacks the ability to resolve fine spectral features and is limited in detailed stellar analysis, low-resolution spectroscopy presents a more efficient option for wide-field observations and rapid data acquisition. Among these, high-quality spectra typically have relatively high signal-to-noise ratios (high-SNR), clear and well-defined spectral lines, and allow for more precise stellar parameter estimation. Low-quality spectra, on the other hand, are characterized by low signal-to-noise ratio (low-SNR), significant noise contamination, blended or poorly defined spectral features, and often lower resolution. These limitations reduce the reliability of parameter extraction and pose challenges for traditional spectral analysis techniques. In this paper, we define low-quality spectra as those with an SNR $\leqslant 15$ in the LAMOST low-resolution spectral data set.

LAMOST is a major astronomical survey project designed to acquire massive stellar spectral data sets. One of its key advantages lies in its ability to obtain spectra for thousands of stars simultaneously in a single exposure, with high spatial coverage and a wide field of view. Since its operation began in 2012, LAMOST has collected over ten million stellar spectra, providing a vast resource for studying stellar atmospheric parameters (Wang et al. 2023). However, the LAMOST data set contains a significant amount of low-quality spectra. These spectra are often characterized by high noise, low-resolution, or poorly defined spectral lines, posing considerable challenges to traditional fitting and line-by-line analysis methods. Low-quality spectra not only reduce the accuracy of atmospheric parameter estimation but also increase the computational burden in large-scale data processing. Therefore, extracting accurate stellar atmospheric parameters from such low-quality spectra has become an urgent and important problem in the field.

1.2. Limitations of Traditional Methods

Traditional approaches for estimating stellar atmospheric parameters primarily rely on spectral line modeling. These include fitting observed spectral features using physical models, or matching observed spectra with synthetic ones generated from theoretical models, in order to infer key parameters such as effective temperature ($T_{\rm eff}$), surface gravity ($\log g$), and metallicity ([X/H]). Such methods typically depend on well-established model atmospheres and extensive synthetic spectral libraries, including MARCS and ATLAS9 (Castelli & Kurucz 2003; Gustafsson et al. 2008). While these techniques can yield accurate parameter estimates under controlled conditions, they become computationally expensive when applied to large-scale spectroscopic surveys. Moreover, their performance is often limited when dealing with low-resolution or low-quality spectra, such as those commonly found in LAMOST observations. In these cases, the accuracy of parameter inference may be significantly degraded due to insufficient spectral detail and noise contamination.

In the past few years, significant progress has been made in the research of stellar atmospheric parameter estimation, involving the application of various methods and techniques. Recio-Blanco et al. (2016) conducted a spectral analysis of the RVS data from the ESA Gaia mission, evaluating the performance of several specialized stellar parameterization codes (such as FERRE, GAUGUIN, and MATISSE). The results showed that these codes are capable of efficiently determining stellar atmospheric parameters. Rajpurohit et al. (2018) utilized high-resolution optical and near-infrared spectra from CARMENES, combined with the BT-Settl synthetic model, to study the method of determining atmospheric parameters of M dwarfs. This study systematically measured the effective temperature, surface gravity, and metallicity of 292 M0 to M9 type M dwarfs, using both visible and near-infrared spectra for the first time. Contursi et al. (2021) optimized the Gaia-ESO line list, improving the match between synthetic and observed spectra, thus laying the

foundation for the accurate determination of stellar atmospheric parameters. Pakhomov (2024) used a specific photometric system and model stellar atmospheres to analyze the accuracy of estimating stellar parameters and color excess from broadband photometry using the χ^2 minimization method. The results indicated that with higher photometric precision, the parameter estimation for cool stars is more accurate, while for hot stars, some parameters have large errors and metallicity could not be determined. Hegedüs et al. (2023) compared the latest data releases from the SDSS-IV APOGEE-2, GALAH, and Gaia-ESO sky surveys, assessing the accuracy and precision of the provided atmospheric parameters and elemental abundances. The study found that, in most cases, there is good agreement between these surveys, but significant differences in elemental abundances were observed, particularly in the absolute abundance scale, providing valuable insights for future sky surveys and atmospheric parameter studies.

However, these methods have certain limitations when handling large-scale data. First, traditional methods typically require detailed physical model fitting for the spectra of each star, which is a complex and computationally expensive process. When dealing with large data sets, these approaches are inefficient and unable to meet the demands for real-time or near-real-time analysis. Moreover, traditional methods have high data quality requirements, as low-SNR or low-resolution spectra can reduce the accuracy of parameter measurements. This is because traditional approaches often rely on detecting and fitting specific absorption lines or spectral features that are easily obscured or distorted in noisy spectra. As a result, they may fail to extract reliable physical parameters when the spectral lines are weak or blended due to noise, making them poorly suited for low-quality data. Therefore, in large-scale spectroscopic surveys, traditional stellar atmospheric parameter measurement methods face limitations in terms of processing efficiency and applicability.

1.3. Advantages of Machine Learning

With the rapid advancement of machine learning technologies—especially the successful applications of deep learning in image recognition and time-series data analysis—machine learning methods have gradually become an important tool for predicting stellar atmospheric parameters. These algorithms can automatically learn the complex nonlinear relationships between inputs and outputs from large data sets, enabling predictions that avoid the traditional dependence on spectral line precision and that can handle noisy or incomplete data.

In the estimation of stellar atmospheric parameters, machine learning offers several notable advantages:

(1) *Efficiency and Large-scale Processing Capability*. Machine learning methods are capable of efficiently training and predicting on massive data sets, significantly improving data processing speed and supporting real-time or near-real-time stellar parameter estimation for large-scale astronomical surveys such as LAMOST and Gaia. Gebran et al. (2022) achieved high-precision results by applying deep learning to derive stellar parameters from observed spectra. Li & Lin (2023) proposed a deep learning model, StarGRUNet, for estimating atmospheric parameters and 13 elemental abundances from LAMOST low-resolution spectra, showcasing the potential of machine learning in processing large-scale astronomical data. Passegger et al. (2020) employed deep neural networks to analyze high-resolution stellar spectra from the CARMENES survey, successfully predicting effective temperature, surface gravity, metallicity, and rotational velocity.

(2) *Nonlinear Relationship Modeling*. The relationship between stellar spectra and atmospheric parameters is often highly nonlinear. Machine learning models, especially deep neural networks, excel at capturing such complex nonlinearities, thereby enhancing estimation accuracy. Giobergia et al. (2023) proposed a multi-objective probabilistic regression approach combining deep learning and inverse modeling techniques to extract atmospheric parameters from exoplanet spectra. Li et al. (2022) developed a multilayer perceptron model capable of efficiently estimating stellar parameters by automatically extracting nonlinear features from spectra with low to medium signal-to-noise ratios (SNRs). Plaza et al. (2023) utilized a one-dimensional (1D) convolutional autoencoder to extract features from spectral data, achieving high-precision interpolation of stellar atmosphere models.

In recent years, deep learning models, especially Convolutional Neural Networks (CNNs), have shown great potential in stellar spectral analysis. Compared to traditional methods, CNNs can automatically extract useful features directly from raw spectral data, avoiding the tedious process of manually selecting or preprocessing spectral features. This allows the model to more efficiently learn the complex nonlinear relationships between spectra and stellar parameters, significantly improving prediction accuracy and efficiency. In the prediction of stellar atmospheric parameters, Xie et al. (2021) proposed a new CNN-based model that can predict the atmospheric parameters of extremely metal-poor stars ([Fe/H] < -2.0 dex) from LAMOST spectra with high precision, including $T_{\rm eff}$, log g, [Fe/H], and [C/Fe], and can distinguish very metal-poor (VMP) stars from ordinary stars with an accuracy of 88.65%. Gebran et al. (2022) proposed a CNN-based deep learning framework to systematically analyze the effects of different hyperparameter combinations on the prediction accuracy of $T_{\rm eff}$, log g, [M/H], and v sin i, pointing out that the requirements for each stellar parameter vary depending on the network architecture. Li et al. (2022) proposed a series of CNNs (GaLNets) to derive the Sérsic profile parameters of galaxies, with GaLNet-2 achieving accuracy comparable to traditional methods and being three

orders of magnitude faster than standard methods, making it suitable for both ground-based and space observations. Shen & Luo (2024) successfully predicted the $T_{\rm eff}$, log g, [Fe/H], absolute magnitude, and color of solar-type stars from LAMOST DR9 low-resolution spectra using CNN, with good accuracy and stability when SNR is greater than 10. Cvrček et al. (2025) combined supervised and unsupervised learning methods and used an autoencoder architecture to analyze HARPS observational data, achieving high-precision stellar parameter predictions (e.g., the average error for $T_{\rm eff}$ is about 50 K, and the errors for [Fe/H] and log g are approximately 0.03 dex and 0.04 dex, respectively), and generating simulated spectra highly similar to the real spectra, demonstrating the application potential of deep generative models in astronomical data compression and reconstruction. Additionally, Olivares et al. (2024) proposed a new algorithm that uses artificial intelligence techniques to automatically estimate the physical parameters of massive stars from a grid of stellar spectral models containing over 573,000 synthetic spectra. The results show that the accuracy of predicting parameters such as effective temperature and surface gravity reached 85%, with an execution time of 6–13 minutes per spectrum, significantly reducing the search time compared to traditional methods. To further reduce the "synthetic gap" between observed spectra and synthetic spectra, Mas-Buitrago et al. (2024) proposed a feature-level deep transfer learning method based on autoencoders, applied to the estimation of $T_{\rm eff}$, log g, [M/H], and v sin i of M dwarfs in the high-resolution CARMENES spectra, significantly reducing the impact of feature distribution differences on model performance.

In summary, although machine learning methods have demonstrated significant advantages in the prediction of stellar atmospheric parameters—particularly in automatic feature extraction, efficient processing of massive data sets, and modeling the nonlinear relationships between spectra and atmospheric parameters, current research primarily focuses on high-quality spectral data. Traditional methods, due to their reliance on high-quality inputs, are often ineffective for low-quality spectra. Similarly, existing machine learning models are mostly designed for high-SNR spectra and lack effective solutions for low-SNR data. Therefore, how to effectively apply machine learning techniques to low-quality spectral data remains an urgent and unresolved challenge. This paper aims to address this issue by exploring machine learning methods suitable for low-quality spectra to improve the accuracy and reliability of stellar atmospheric parameter predictions.

1.4. Contributions and Structure of This Study

The primary objective of this study is to enhance the prediction accuracy of stellar atmospheric parameters—namely, effective temperature ($T_{\rm eff}$), surface gravity (log g), and metallicity ([Fe/H])—from low-quality LAMOST stellar spectra using machine learning techniques. The main innovations of this work can be summarized in the following three aspects:

1. First, we propose a Cycle-CNN algorithm for the estimation of stellar atmospheric parameters. By incorporating the cycle-consistency learning mechanism from Cycle-GAN, the model establishes a forward mapping from low-quality spectra to atmospheric parameters and a backward mapping from parameters to spectra. This dual-mapping design effectively mitigates overfitting in small-sample conditions and enhances the model's stability and generalization capability.
2. Second, the proposed method achieves high-precision predictions of stellar atmospheric parameters even under extremely low-SNR conditions. Experimental results on LAMOST DR9 spectra across various SNR intervals show that the model performs robustly in estimating effective temperature, surface gravity, and metallicity, even when SNR is as low as 2–5.
3. Third, the proposed method can be employed to supplement missing atmospheric parameters in low-quality spectra within the LAMOST database, thereby improving the scientific utility of such spectral data.

This paper is organized as follows. The proposed method is introduced in Section 2. The data are described in Section 3, and the proposed method is evaluated through prediction results and compared with the results from other surveys in Section 4. The discussion and conclusion are presented in Section 5.

2. Method

Cycle-GANs introduce the concept of cycle consistency loss, which allows images to be translated back and forth between two domains while maintaining semantic consistency (Zhu et al. 2017). This mechanism enables learning domain mappings without requiring paired data, and has been widely adopted in applications such as image style transfer and domain adaptation.

Inspired by this idea, we propose a Cycle-CNN framework for stellar atmospheric parameter estimation. The model takes a stellar spectrum image as input and predicts three physical parameters: effective temperature ($T_{\rm eff}$), surface gravity (log g), and metallicity ([Fe/H]). To enhance the robustness and accuracy of parameter estimation, we introduce a cycle consistency constraint: the predicted parameters are fed into a decoder that reconstructs a synthetic spectrum, which is then compared with the original input. This encourages the encoder to generate physically meaningful representations.

To further strengthen feature extraction and reconstruction capabilities, we incorporate Squeeze-and-Excitation (SE)

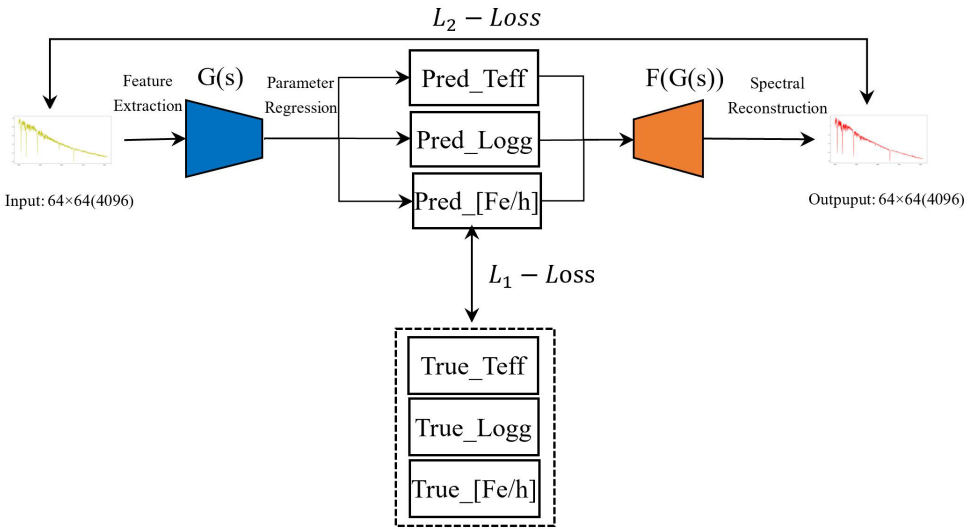


Figure 1. Overview of the Cycle-CNN framework. The encoder extracts atmospheric parameters from spectral images, and the decoder reconstructs spectra based on the predicted parameters.

attention modules into both the encoder and decoder. These modules adaptively recalibrate channel-wise feature responses, enhancing the model's expressiveness. The overall architecture of the Cycle-CNN is illustrated in Figure 1.

2.1. Network Architecture

The encoder and decoder structures are visually illustrated in Figures 2 and 3, respectively. Table 1 presents the detailed architecture of the encoder and decoder components.

2.2. Network Components

The main components used in the encoder and decoder are briefly described below:

1. *Conv2D*. Applies two-dimensional (2D) convolution to extract local spatial features from spectral images. Used in the encoder to hierarchically encode input information.
2. *ReLU*. The rectified linear unit activation function, $\mathrm{ReLU}(x) = \max(0, x)$, introduces nonlinearity and improves training efficiency.
3. *SE Module*. The SE block recalibrates channel-wise feature responses using global pooling and attention. This enhances the model's ability to focus on informative spectral features.
4. *MaxPooling*. Reduces spatial dimensions via 2×2 pooling, preserving dominant activations while lowering computational complexity.
5. *Flatten*. Converts 3D feature maps into 1D vectors, enabling connection to fully connected layers.
6. *Dense*. Fully connected layers for dimensionality transformation. Used for both parameter regression (encoder) and latent vector expansion (decoder).
7. *Reshape*. Used to reshape the expanded latent vector into a tensor suitable for transposed convolution.
8. *Conv2DTranspose*. Also known as deconvolution. Upsamples spatial resolution using learnable filters. Used in the decoder to reconstruct the spectral image from feature maps.

2.3. Loss Function

The total loss function combines two terms: atmospheric parameter loss and spectral reconstruction loss.

1. *Atmospheric Parameter Loss*. Measures the error between predicted and ground truth stellar parameters using mean absolute error (MAE):

$$L_{\mathrm{atm}}(G) = \mathbb{E}_{s\sim p_{\mathrm{data}}(s)}[||G(s) - p_{\mathrm{true}}||_1]. \quad (1)$$

2. *Spectral Reconstruction Loss*. Measures the deviation between the reconstructed spectrum and the original input using mean squared error:

$$L_{\mathrm{spec}}(F, G) = \mathbb{E}_{s\sim p_{\mathrm{data}}(s)}[||F(G(s)) - s||_2^2]. \quad (2)$$

The final objective function is

$$L_{\mathrm{total}} = L_{\mathrm{atm}} + \lambda L_{\mathrm{spec}}, \quad (3)$$

where λ is a hyperparameter that balances the two loss terms.

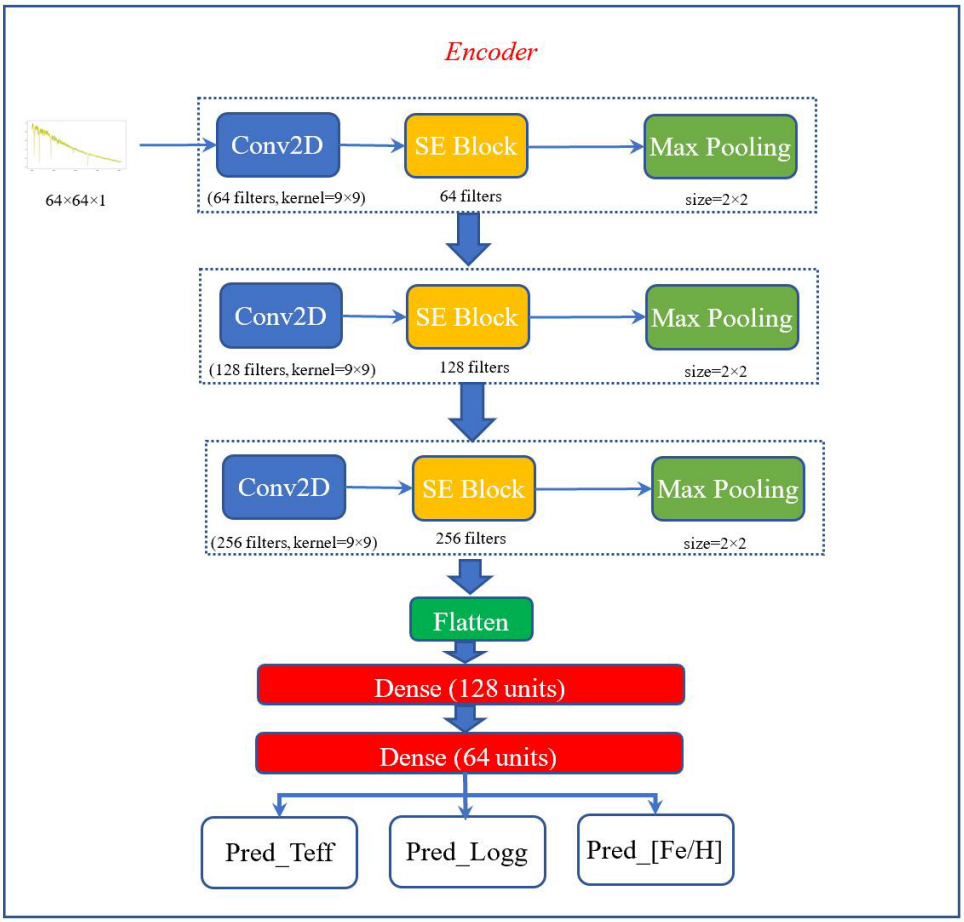


Figure 2. Encoder structure diagram.

2.4. Differences between Cycle-CNN and Cycle-GAN

Although our proposed method draws inspiration from Cycle-GAN through its adoption of the cycle-consistency principle, it fundamentally differs from Cycle-GAN in both architectural design and training objectives.

Cycle-GAN employs adversarial training involving a discriminator to encourage the generated data distribution to match the real one. In contrast, our Cycle-CNN model does not include a discriminator. Instead, the training process is supervised and relies on paired data, making the model more stable and easier to optimize. In our framework, the encoder functions as a regression module that predicts stellar atmospheric parameters (e.g., $T_{\rm eff}$, log g, [Fe/H]), while the decoder reconstructs the input spectrum from the predicted parameters.

Cycle-CNN inherits the core idea of cycle consistency from Cycle-GAN but discards the adversarial component in favor of a physically grounded supervised learning scheme. The use of cycle consistency ensures that the predicted atmospheric parameters can be used to reconstruct the original input spectrum, thereby enhancing the model's robustness, interpretability, and physical plausibility. This architectural and methodological divergence ensures that the model is robust, interpretable, and well-suited for regression tasks in stellar parameter estimation—without incurring the risks or complexities associated with adversarial training frameworks.

The training process uses the Adam optimizer with an initial learning rate set to 5×10^{-4}. The learning rate scheduling strategy adopts `ReduceLROnPlateau`, which automatically reduces the learning rate to 0.5 times its current value if the validation loss does not improve for 10 consecutive epochs. The hyperparameter $\lambda_{\rm recon}$ in the total loss function is empirically set to 0.5. The entire model is trained for a total of 300 epochs. Early stopping is applied, and training is terminated early if the validation loss does not improve within 20 epochs. In addition, the data set is split as follows: 80% for the training and validation set, and 20% for the test set. Among the training data, 20% is further used as the validation set.

3. Data

High-resolution spectra are widely utilized to determine the physical and chemical properties of benchmark stars with great

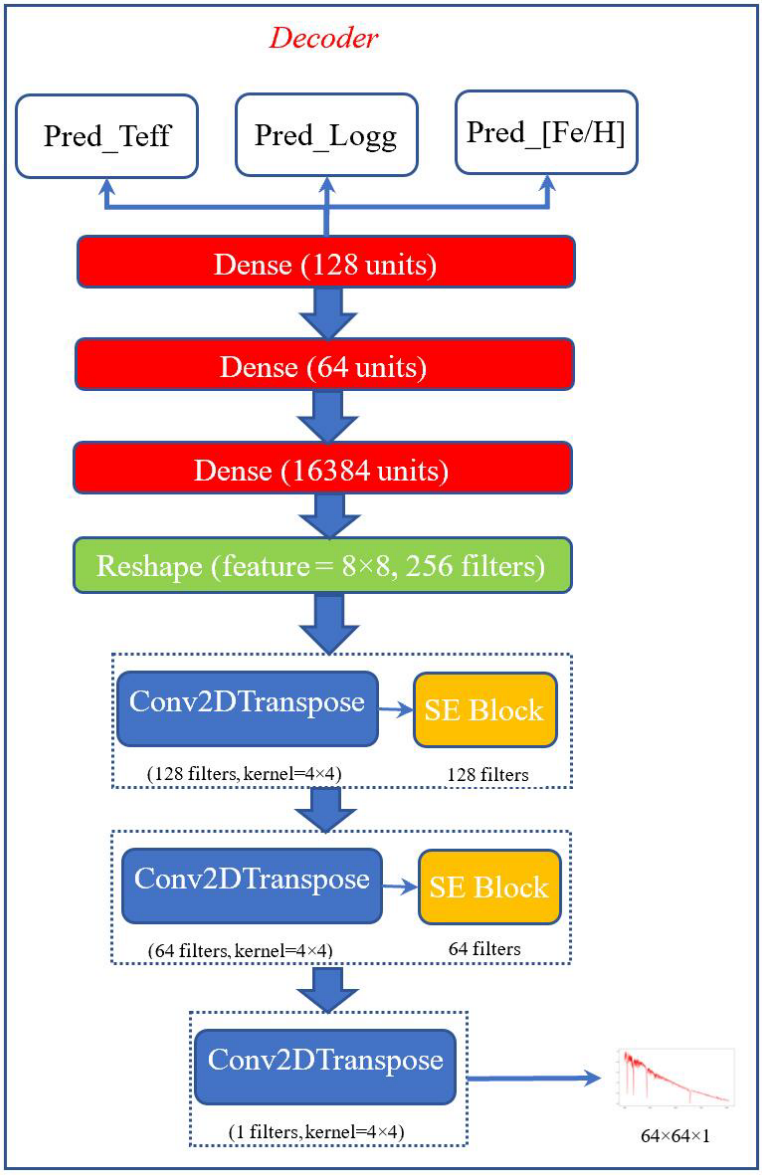


Figure 3. Decoder structure diagram.

precision. Owing to their ability to capture intricate spectral features, they serve as powerful tools for constraining theoretical models and deriving accurate stellar parameters and elemental abundances. Nevertheless, the acquisition of such data is resource-intensive, as it demands prolonged exposure times and optimal observing conditions, making large-scale high-resolution spectroscopic surveys costly and less feasible. In contrast, recent advances in deep learning have emerged as a promising alternative, providing essential methodological support for large-scale low-resolution surveys, including multi-object fiber spectroscopy programs such as LAMOST, Subaru PFS, and 4MOST.

The LAMOST project aims to conduct unprecedented large-scale spectroscopic surveys to address the global shortage of spectral data. The telescope is located at the Xinglong Station of the National Astronomical Observatories, Chinese Academy of Sciences, situated on the southern slope of the main peak of the Yanshan Mountains, in Lianyingzhai, Xinglong County, Hebei Province (longitude 117°50′E, latitude 40°23′N), at an altitude of 960 m. LAMOST adopts a unique meridian reflecting Schmidt design, offering a wide field of view up to 5° and lying horizontally along the north-south direction. Combined with active optics technology, it achieves highly efficient spectral acquisition. The optical system consists of three main components: the reflecting Schmidt corrector mirror (MA), the spherical primary mirror (MB), and the focal plane fiber array. The MA is composed

Table 1
Architecture of the Encoder and Decoder

Stage	Operation	Output Shape	Parameters/Notes
Encoder	Input	64 × 64 × 1	Spectral image input
	Conv Block 1	32 × 32 × 64	64 filters, 9 × 9, SE(64), pool 2 × 2
	Conv Block 2	16 × 16 × 128	128 filters, 9 × 9, SE(128), pool 2 × 2
	Conv Block 3	8 × 8 × 256	256 filters, 9 × 9, SE(256), pool 2 × 2
	Flatten	16,384	Flattened feature map
	Dense 1	128	⋯
	Dense 2	64	⋯
	Output	3	$T_{\rm eff}$, log g, [Fe/H]
Decoder	Input	3	Atmospheric parameter vector
	Dense 1	64	⋯
	Dense 2	128	⋯
	Dense 3	16,384	To be reshaped
	Reshape	8 × 8 × 256	⋯
	Deconv 1	16 × 16 × 128	128 filters, 4 × 4, stride 2, SE(128)
	Deconv 2	32 × 32 × 64	64 filters, 4 × 4, stride 2, SE(64)
	Deconv 3	64 × 64 × 1	1 filter, 4 × 4, stride 2

of 24 hexagonal flat sub-mirrors (5.72 m × 4.4 m), which can be adjusted in real time according to observational needs. The MB is formed by splicing 37 spherical sub-mirrors (6.67 m × 6.05 m), focusing the incoming light to form high-quality imaging. LAMOST's effective aperture can dynamically vary from 3.6 to 4.9 m depending on the observed sky area. At the focal plane, 4000 auto-positioning fibers are installed, each connected to one of 16 spectrographs, enabling the simultaneous acquisition of spectra from 4000 celestial objects. This makes LAMOST the world's most efficient optical telescope in terms of spectral acquisition rate and survey capability. It plays a significant role in studies of Galactic structure, stellar formation and evolution, and active galactic nuclei (Zhao 2014).

This study employs low-resolution ($R \approx 1800$) stellar spectra from the ninth data release (LAMOST DR9) of the LAMOST survey, which was publicly released as LAMOST DR9 (V2) on 2023 September 28. This release includes observational data collected from 2011 October to 2021 June and comprises both low-resolution and medium-resolution spectral data. The LAMOST DR9 data set (V2) contains a total of 19.45 million spectra, along with 8.61 million sets of stellar spectral parameters, of which 10.81 million are low-resolution spectra. Among these, approximately 3.31 million stellar spectra exhibit an SNR lower than 10. When the SNR is low, spectral quality may be degraded, manifesting as issues such as flux gaps, abnormal stitching, and other artifacts. Moreover, a substantial proportion of these low-quality spectra also suffer from missing parameters. The presence of such low-quality spectra may adversely affect subsequent scientific analyses and investigations.

In this study, the original data were grouped and filtered based on the SNR in the g-band ($\rm SNR_g$) of the spectra. The continuum-normalized spectral data provided directly by LAMOST DR9 were used, and the samples were divided into three SNR intervals: 10–15 (Data Set1), 5–10 (Data Set2), and 2–5 (Data Set3). During the data filtering process, the following exclusion criteria were applied to ensure the validity and consistency of the physical parameters:

1. Records with a redshift value (z) of −9999 were excluded;
2. Records with missing values in effective temperature ($T_{\rm eff}$), surface gravity (log g), or metallicity ([Fe/H]) were removed.

Based on the above filtering criteria, three SNR-based data sets that meet the requirements were obtained, as summarized in Table 2. To maintain consistency in sample size, 60,000 samples were randomly selected using simple random sampling from both Data Set1 and Data Set2. However, due to the limited number of samples with SNR in the range of 2–5, only 3067 samples in Data Set3 satisfied the filtering criteria. Therefore, all available samples in Data Set3 were used in the subsequent experiments. These selected samples were split into training, testing, and validation sets as described in the final paragraph of Section 2, with 80% allocated to training, 20% to testing, and 20% of the training set further separated as validation.

The stellar atmospheric parameters used in this study include $T_{\rm eff}$, log g, and [Fe/H]. Their value ranges across the data sets are summarized in Table 3.

To avoid issues caused by scale differences between dimensions in the input data, preprocessing was applied prior to the use of machine learning methods. This preprocessing included redshift removal (i.e., radial velocity correction) and standardization of the training data. No further data processing was performed.

3.1. Redshift Removal

Due to stellar motions, observed spectra may experience Doppler redshifts. Therefore, it is essential to correct for radial velocity to align all spectra to a common reference frame. In this study, Equation (4) was used for the correction

$$\lambda_{\rm rest} = \frac{\lambda_{\rm obs}}{1+z}, \tag{4}$$

where:

1. $\lambda_{\rm obs}$ is the observed wavelength (affected by redshift);
2. $\lambda_{\rm rest}$ is the rest-frame wavelength;

Table 2
Statistics of Selected LAMOST DR9 Spectra by SNR_g Range

Data Set	SNR Range	Total Samples
Data Set1	10–15	60,000
Data Set2	5–10	60,000
Data Set3	2–5	3067

Table 3
Adopted Parameter Ranges for Different Sets

Set	Parameter	Effective Parameter Range
Data Set1	FeH	$-2.469 \sim 0.954$
	Log g	$0.065 \sim 4.899$
	$T_{\rm eff}$	$3809.58 \sim 12515.7$
Data Set2	FeH	$-2.494 \sim 0.918$
	Log g	$0.102 \sim 4.9$
	$T_{\rm eff}$	$3789.04 \sim 11318.0$
Data Set3	FeH	$-2.286 \sim 0.811$
	Log g	$0.254 \sim 4.9$
	$T_{\rm eff}$	$3782.9 \sim 7826.76$

3. z is the redshift value.

3.2. Data Normalization

The LAMOST spectra cover the wavelength range from 3700 to 9100 Å. In this work, we restrict the wavelength range to 4000–8096 Å. Within this range, the spectra are resampled using interpolation at 1 Å intervals.

Based on experimental comparisons, we found that applying min–max normalization to spectral fluxes and z-score normalization (zero mean, unit variance) to stellar labels yields the best results in model training and prediction.

For the training set, let there be m stellar spectra, each with n pixels. Denote $F_{i,j}$ as the flux value at the jth pixel of the ith spectrum. First, the global minimum and maximum flux values across all spectra are computed by Equation (5)

$$F_{\rm min} = \min_{i,j}\{F_{i,j}\}, \quad F_{\rm max} = \max_{i,j}\{F_{i,j}\}. \tag{5}$$

Then, the min–max normalization is applied to each pixel using Equation (6)

$$f_{i,j} = \frac{F_{i,j} - F_{\rm min}}{F_{\rm max} - F_{\rm min}}. \tag{6}$$

Stellar labels (e.g., $T_{\rm eff}$, log g, [Fe/H]) are normalized using Equation (7). Each label L is normalized individually based on its mean μ and standard deviation (STD) σ in the training set

$$l = \frac{L - \mu}{\sigma}. \tag{7}$$

During the prediction phase, the normalized outputs are transformed back to their physical values using Equation (8)

$$L = l \cdot \sigma + \mu. \tag{8}$$

In addition, we trained individual models on each SNR-based data set (Data Set1, Data Set2, and Data Set3) rather than using a unified model. This approach ensures that the model is specifically optimized for different noise levels.

4. Experimental Results and Comparisons

4.1. Prediction Results of Stellar Atmospheric Parameters from LAMOST DR9

Figure 4 presents six subplots showing the prediction performance of our model on Data Set1 (SNR = 10–15). The top row illustrates the 1:1 correspondence heatmaps between the predicted and true values of $T_{\rm eff}$, log g, and [Fe/H], from left to right respectively, while the bottom row shows the prediction errors as functions of the true values. The predictions of $T_{\rm eff}$ demonstrate good overall agreement, with MAE of 63.22 K and STD of 92.47 K, indicating good performance. For log g, the MAE is 0.11 dex and the STD is 0.16 dex. However, a noticeable bimodal structure is observed, which may stem from the imbalance in stellar types (mainly red giants and main-sequence stars) in the data set. The [Fe/H] predictions yield an MAE of 0.07 dex and an STD of 0.10 dex, also reflecting good accuracy, although predictions in the low-metallicity region ([Fe/H] < -1.0 dex) are sparse and scattered due to the limited number of such stars in the training set.

Similarly, Figure 5 presents six subplots showing the prediction results on Data Set2 (SNR = 5–10). The $T_{\rm eff}$ predictions achieve an MAE of 89.45 K and an STD of 122.55 K, still indicating good overall consistency. The error distribution shows small deviations in the 4000–7000 K range, with only a slight divergence at the high-temperature end. The log g predictions yield an MAE of 0.17 dex and an STD of 0.24 dex. As shown in the middle panels, the model maintains relatively high accuracy in the high-gravity regime (log $g > 3.5$), which mainly corresponds to main-sequence stars. However, systematic underestimation becomes evident for lower gravity values, particularly below log $g < 2.5$, where many red giant stars reside. The error distribution shows a clear shift, suggesting the model tends to bias toward higher surface gravities in this range. This behavior may be attributed to the imbalance of training samples, where low-gravity stars are underrepresented and exhibit broader spectral degeneracies. The [Fe/H] prediction results yield the MAE of 0.11 dex and STD of 0.15 dex, with a good fit in the range $-0.5 <$ [Fe/

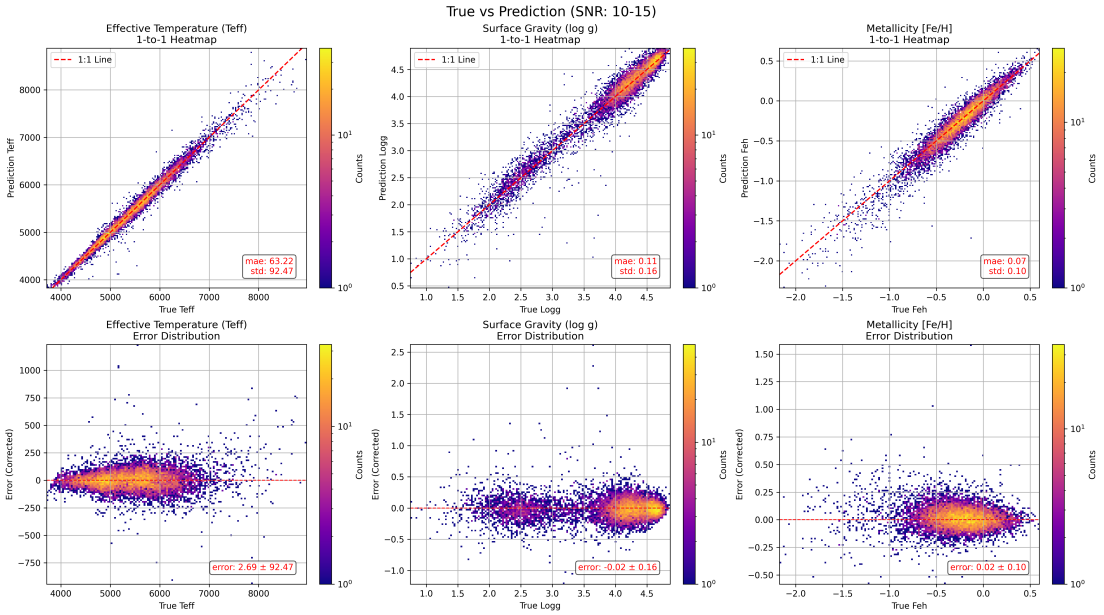


Figure 4. Prediction performance on Data Set1 (SNR = 10–15): Comparison between predicted and true stellar atmospheric parameters ($T_{\rm eff}$, log g, and [Fe/H]). The top row shows 1:1 correspondence heatmaps; the bottom row shows prediction errors as functions of the true values.

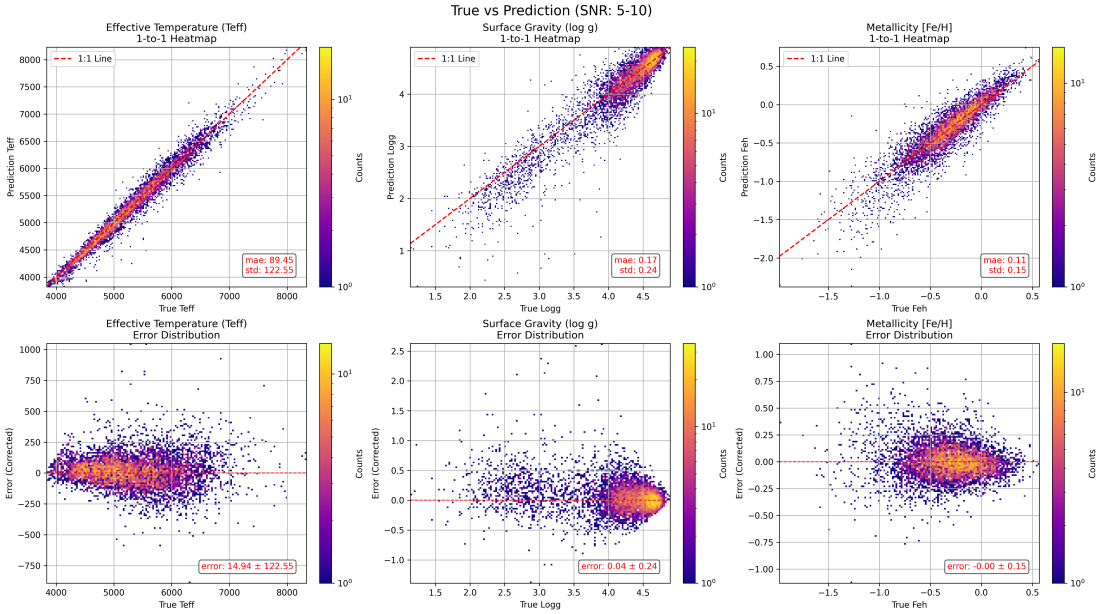


Figure 5. Similar to Figure 4, the prediction performance on Data Set2. The top row shows 1:1 correspondence heatmaps; the bottom row shows prediction errors as functions of the true values.

H] $<$ 0.2 dex. In extremely low-metallicity regions ([Fe/H] $<$ -1.0 dex), the predictions become more dispersed, primarily due to the limited number of training examples and weaker metal absorption features in such spectra. Nevertheless, the predictions of the three atmospheric parameters remain consistently stable in this data set, indicating strong noise tolerance of the model.

Figure 6 shows six subplots for Data Set3 (SNR = 2–5), which represents a challenging scenario as the SNR is extremely low. Compared to Figures 4 and 5, the overall prediction accuracy decreases significantly, and the point clouds become more scattered, highlighting the difficulty of regressing stellar parameters from very low-quality spectra. For $T_{\rm eff}$, the MAE is 145.36 K and the STD is 212.25 K. While

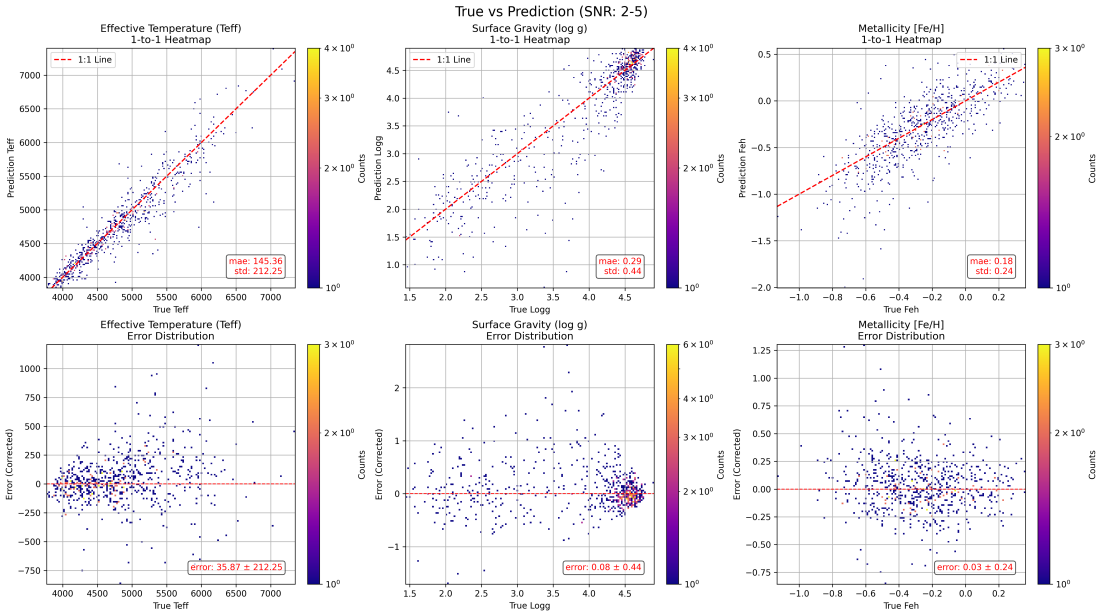


Figure 6. Similar to Figure 4, the prediction performance on Data Set3. The top row shows 1:1 correspondence heatmaps; the bottom row shows prediction errors as functions of the true values.

most points remain near the diagonal in the 1:1 plot, a systematic overestimation is observed in the 5000–6500 K region. The log g predictions show the MAE of 0.29 dex and STD of 0.44 dex. The points are relatively concentrated in the $\log g > 4.0$ region, but become sparse and highly variable for $\log g < 3.0$. The [Fe/H] results yield the MAE of 0.18 dex and STD of 0.24 dex. While predictions for [Fe/H] > -0.5 dex remain acceptable, the point cloud becomes notably sparse and dispersed in the low-metallicity region ([Fe/H] < -1.0 dex). This is primarily due to two factors: the extremely low-SNR spectra, which blur spectral features, and the limited number of training samples in this range (only 3067 spectra), which hampers model generalization. Nonetheless, our method still maintains reasonable prediction accuracy.

From these results, it can be seen that Data Set1 and Data Set2 yield lower MAE and STD values with predictions closely aligned along the diagonal, indicating high accuracy. While the model exhibits greater prediction errors on Data Set3 relative to Data Set1 and Data Set2, its outputs remain within a reasonable range. These results demonstrate that although the prediction accuracy of atmospheric parameters decreases with spectral quality, our model retains a certain degree of robustness even for extremely low-SNR spectra.

4.2. Comparison with APOGEE

To evaluate the performance of our method across different SNR ranges, we cross-matched the predicted results with the spectra in the APOGEE DR17 catalog. The cross-matching results for the three data sets, Data Set1, Data Set2, and Data Set3, yielded 727, 189, and 25 matched spectra, respectively. The results are shown in Figures 7, 8, and 9. In each figure, the top panels display the 1:1 comparison between the predicted values and the APOGEE ones, while the bottom panels show the residual distributions as functions of the predicted values. From left to right, the subplots correspond to effective temperature ($T_{\rm eff}$), surface gravity (log g), and metallicity ([Fe/H]).

As shown in Figure 7, within Data Set1 (SNR = 10–15), the predicted parameters exhibit good agreement with the APOGEE values. The bias in $T_{\rm eff}$ is -12.92 K, with a dispersion of 147.76 K, indicating that the overall predictions are unbiased, with only a moderate degree of scatter. The residuals are approximately symmetrically distributed, although there is slight broadening in the low-temperature region. The predicted log g values are also generally consistent with the reference values, showing a bias of -0.09 dex and a dispersion of 0.27 dex. The error distribution appears to be largely random, without any significant systematic trends. For [Fe/H], the prediction results are stable, with a bias of 0.00 dex and a dispersion of only 0.14 dex, which also demonstrates good consistency.

As shown in Figure 8, within Data Set2 (SNR = 5–10), the model performance slightly degrades but remains acceptable. The bias in $T_{\rm eff}$ possibly increases to -15.45 K, while the dispersion decreases to 128.54 K. This may be because the estimation of $T_{\rm eff}$ relies heavily on the continuum shape and temperature-sensitive lines like the Balmer Hα line, which can be partially obscured by noise at this SNR. As a result, the model might rely more on the continuum trend, which is generally more robust to noise but may introduce systematic bias, such as misestimating the continuum slope. The suppression of high-frequency noise could cause

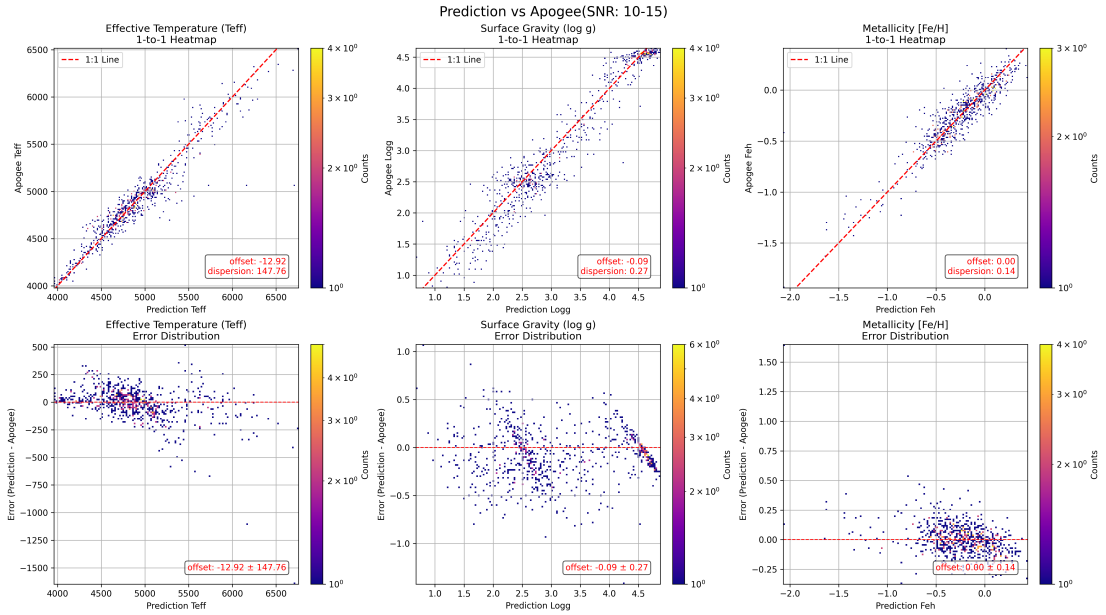


Figure 7. Comparison of predicted stellar parameters with APOGEE values in the SNR 10–15 range. The top panels show the 1:1 correspondence between predictions and reference values; the bottom panels show residual distributions for $T_{\rm eff}$, log g, and [Fe/H], from left to right respectively.

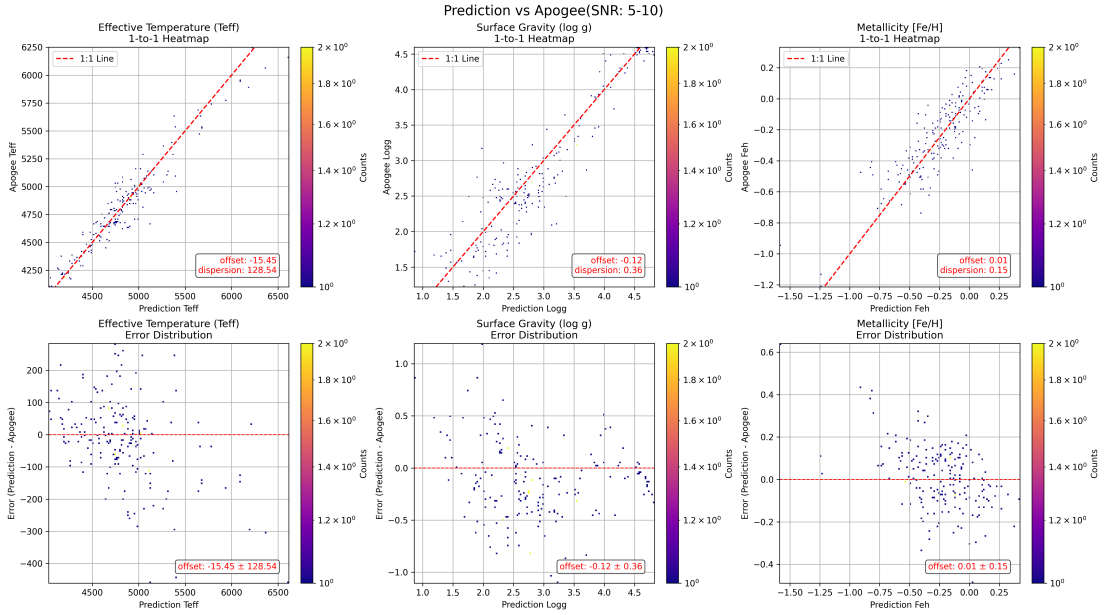


Figure 8. Comparison of predicted stellar parameters with APOGEE values in the SNR 5–10 range. The top panels show the 1:1 correspondence between predictions and reference values; the bottom panels show residual distributions for $T_{\rm eff}$, log g, and [Fe/H], from left to right respectively.

predictions to cluster near the average temperature distribution in the training set (around 4000–7000 K), reducing dispersion but increasing bias. Additionally, the reconstruction loss in Cycle-CNN may encourage predictions to stay close to the training mean, further lowering dispersion at the cost of absolute accuracy. The bias in log g appears to increase to −0.12 dex with a dispersion of 0.36 dex, showing larger scatter in the low-gravity region. Predictions of [Fe/H] remain stable, with a bias of 0.01 dex and dispersion of 0.15 dex. This might be because log g and [Fe/H] depend on more robust spectral features—such as pressure-sensitive lines (e.g., Mg triplet, Ca II) for log g and metal lines (e.g., Fe I) for [Fe/H]—and have more uniform sample distributions in training, which could prevent a similar inverse trend between bias and dispersion as seen for $T_{\rm eff}$.

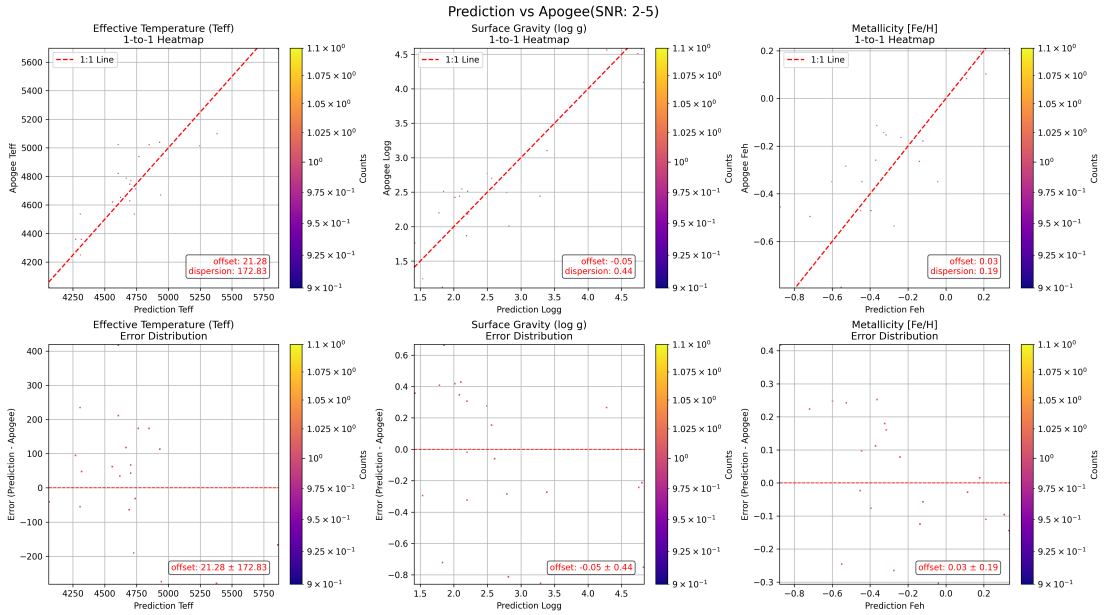


Figure 9. Comparison of predicted stellar parameters with APOGEE values in the SNR 2–5 range. The top panels show the 1:1 correspondence between predictions and reference values; the bottom panels show residual distributions for $T_{\rm eff}$, log g, and [Fe/H], from left to right respectively.

As shown in Figure 9, in Data Set3 (extremely low-SNR range of 2–5), only 25 spectra are available for evaluation, resulting in large statistical uncertainties. Despite this limitation, the predicted $T_{\rm eff}$ shows a bias of 21.28 K with a dispersion of 172.83 K, indicating that the model's ability to constrain temperature significantly weakens at such low SNR levels. The bias in log g is −0.05 dex, but the dispersion increases to 0.44 dex, with some outliers observed. These outliers can be attributed primarily to the extremely limited number of training samples in the low surface gravity region (log,$g < 3.0$). Such sparsity in the parameter space reduces the model's generalization ability and increases the likelihood of poor predictions in these areas. In contrast, [Fe/H] continues to exhibit good predictive accuracy, with a bias of 0.03 dex and a dispersion of 0.19 dex. Although the evaluation sample size is small, the predicted values remain closely concentrated around the 1:1 line.

Overall, our method demonstrates strong robustness in predicting stellar atmospheric parameters from low-SNR spectra. In particular, the predictions of metallicity ([Fe/H]) remain highly accurate, showing only minimal bias and low dispersion even under conditions where SNR < 5. As expected, the predictive accuracy of $T_{\rm eff}$ and log g slightly declines with decreasing SNR; however, the overall performance remains within an acceptable range for astrophysical research. These results indicate that our algorithm can provide reliable estimates of stellar atmospheric parameters even when the available spectral data are limited.

5. Discussion and Conclusion

In this paper, we propose a novel Cycle-CNN algorithm for predicting stellar atmospheric parameters from low-resolution, low-SNR spectra in the LAMOST DR9 survey. This method combines Cycle-GANs with CNN, and incorporates the SE block to enhance the representation capability of feature channels. The spectra are first mapped to atmospheric parameters and then reversed back to spectra. This cycle-consistent process effectively prevents overfitting and model collapse. The design ensures that the model can still accurately infer atmospheric parameters for giant stars even with limited data.

Experiments show that the proposed method exhibits strong robustness under different SNR conditions. Within the SNR range of 10–15 (Data Set1), the proposed method outputs are highly consistent with the ground truth, with low MAE and STD for all three parameters. In the SNR range of 5–10 (Data Set2), the performance degrades slightly but remains within acceptable limits. Even under extremely low-SNR range of 2–5 (Data Set3), the proposed method maintains reasonable predictive performance, especially for metallicity ([Fe/H]), which is less sensitive to noise and shows greater stability compared to $T_{\rm eff}$ and log g.

To further validate the robustness of the proposed method, we conducted a cross-match between our predicted parameters and the APOGEE DR17 catalog. For spectra within Data Set1, the predictions for effective temperature ($T_{\rm eff}$), surface gravity (log g), and metallicity ([Fe/H]) show excellent agreement

with APOGEE values, featuring minimal bias and low dispersion. As SNR decreases (Data Set2 and Data Set3), the model's performance in predicting $T_{\rm eff}$ and $\log g$ experiences slight degradation, as expected, particularly in low-temperature and low-gravity regimes. However, the predictions remain within an acceptable error margin. Notably, the metallicity estimates remain remarkably stable and accurate even at SNR < 5, with biases near zero and minimal dispersion. These results demonstrate that the proposed method not only aligns well with internal labels but also agrees with high-quality external survey data.

Nevertheless, our method still has the following limitations:

1. *Limited coverage of the training parameter space*. The performance of data-driven models heavily relies on the representativeness of the training set. If certain types of stars are underrepresented or missing—such as extremely hot, cool, metal-rich, or metal-poor stars—the model may lack the ability to make accurate predictions in those regions of the parameter space.
2. *Imbalanced distribution in training data*. Stars located at the boundaries of the parameter space tend to be scarce in the data set. These edge cases are essential for defining the model's extrapolation capacity, but due to their limited number, they have a reduced influence on loss optimization during training, potentially leading to lower prediction accuracy in those regions.
3. *Uncertainty in spectral parameters*. The stellar atmospheric parameters used for training, which are derived from LAMOST, carry inherent observational uncertainties. These uncertainties are not explicitly modeled during training, which may result in underestimated uncertainty in the final predictions.

Despite these challenges, our results indicate that Cycle-CNN can effectively improve the accuracy of atmospheric parameter estimation from low-resolution, low-SNR stellar spectra in LAMOST, thereby enhancing the overall utility of spectroscopic data.

Acknowledgments

This work is supported by the Natural Science Foundation of Shandong Province (Nos. ZR2022MA076 and ZR2024MA063), the National Natural Science Foundation of China (NSFC, grant Nos. 11873037, U1931209, and 11803016), the science research grants from the China Manned Space Project with No. CMS-CSST-2021-B05 and CMS-CSST-2021-A08, and is partially supported by the Doctoral Research Foundation of Shandong Technology and Business University (grant No. 306519) and the Young Scholars Program of Shandong University, Weihai (2016WHWLJH09). This research has made use of data products from LAMOST. The Guo Shou Jing Telescope (the Large Sky Area Multi-Object Fiber Spectroscopic Telescope, LAMOST) is a National Major Scientific Project built by the Chinese Academy of Sciences. Funding for the project has been provided by the National Development and Reform Commission. LAMOST is operated and managed by National Astronomical Observatories, Chinese Academy of Sciences.

References

Castelli, F., & Kurucz, R. L. 2003, in IAU Symposium 210, Modelling of Stellar Atmospheres, ed. N. Piskunov, W. W. Weiss, & D. F. Gray, A20
Contursi, G., de Laverny, P., Recio-Blanco, A., et al. 2021, A&A, 654, A130
Cvrček, V., Romaniello, M., Šára, R., et al. 2025, A&A, 693, A256
DESI Collaboration, Aghamousa, A., Aguilar, J., et al. 2016, arXiv:1611.00036
Gebran, M., Connick, K., Farhat, H., et al. 2022, OAst, 31, 38
Giobergia, F., Koudounas, A., & Baralis, E. 2023, in Proc. of the 17th Int. Conf. on Application of Information and Communication Technologies (AICT), 1 (Piscataway, NJ: IEEE),
Gustafsson, B., Edvardsson, B., Eriksson, K., et al. 2008, A&A, 486, 951
Hegedüs, V., Mészáros, S., Jofré, P., et al. 2023, A&A, 670, A107
Ho, A. Y. Q., Ness, M. K., Hogg, D. W., et al. 2017, ApJ, 836, 5
Li, R., Napolitano, N. R., Roy, N., et al. 2022, ApJ, 929, 152
Li, X., & Lin, B. 2023, MNRAS, 521, 6354
Li, X., Wang, Z., Zeng, S., et al. 2022, RAA, 22, 065018
Luo, A.-L., Zhao, Y.-H., Zhao, G., et al. 2015, RAA, 15, 1095
Majewski, S. R., Schiavon, R. P., Frinchaboy, P. M., et al. 2017, AJ, 154, 94
Mas-Buitrago, P., González-Marcos, A., Solano, E., et al. 2024, A&A, 687, A205
Olivares, E., Curé, M., Araya, I., et al. 2024, Mathematics, 12, 3169
Pakhomov, Y. V. 2024, AstL, 50, 34
Passegger, V. M., Bello-García, A., Ordieres-Meré, J., et al. 2020, A&A, 642, A22
Plaza, C. W., Ramos, A. A., & Prieto, C. A. 2023, A&A, 675, A191
Prusti, T., de Bruijne, J. H. J., Brown, A. G. A., et al. 2016, A&A, 595, A1
Rajpurohit, A. S., Allard, F., Rajpurohit, S., et al. 2018, A&A, 620, A180
Recio-Blanco, A., De Laverny, P., Prieto, C. A., et al. 2016, A&A, 585, A93
Ricker, G. R., Winn, J. N., Vanderspek, R., et al. 2015, JATIS, 1, 014003
Shen, Y. Y., & Luo, A. L. 2024, A&A, 691, A218
Wang, J., Cao, Z., Huang, Y., et al. 2023, RAA, 23, 025020
Xie, J., Bu, Y., Liang, J., et al. 2021, AJ, 162, 155
York, D. G., Adelman, J., Anderson, J. E., et al. 2000, AJ, 120, 1579
Zhao, Y. 2014, Proc. SPIE, 9145, 439
Zhu, J. Y., Park, T., Isola, P., et al. 2017, in 2017 IEEE Int. Conf. on Computer Vision (ICCV) (Venice, Italy: IEEE), 2242